Lkhamsuren Bayarjargal* and Björn Winkler

Second harmonic generation measurements at high pressures on powder samples

Abstract: This article reviews the most recent results concerning second harmonic generation (SHG) experiments of non-phase matchable and phase matchable powder samples at high pressures and explains the pressure dependence of the intensity of the SHG signal by correlating it to the ratio between the average coherence length and the average particle size. The examples discussed here include pressure-induced structural changes in quartz, ZnO, ice VII and KIO_3. It is shown that the second harmonic generation technique is a unique tool for the detection of pressure-induced structural phase transitions. It is laboratory based and allows fast measurements. It is complementary to X-ray diffraction and provides additional information about the presence of an inversion center for unknown or controversially discussed structures at high pressure.

Keywords: high pressure, phase transition, second harmonic generation

*Corresponding Author: **Dr. Lkhamsuren Bayarjargal,** Institut für Geowissenschaften, Goethe-Universität, Altenhöferallee, 1, 60438 Frankfurt a. M., Germany, Tel.: +49-69-79840106, Fax: +49-69-79840109, e-mail: Bayarjargal@kristall.uni-frankfurt.de
Prof. Dr. Björn Winkler: Institut für Geowissenschaften, Goethe-Universität, Altenhöferallee, 1, 60438 Frankfurt a. M., Germany, Tel.: +49-69-79840107, Fax: +49-69-79840109, e-mail: B.Winkler@kristall.uni-frankfurt.de

1 Introduction

If the intense electromagnetic field of a laser interacts with a crystal, the dielectric polarization of a crystal ceases to be a linear response of the incident electric field, and new effects appear. Second harmonic generation (SHG), i.e. the creation of a photon with twice the frequency of two incident photons, was the first nonlinear optical phenomena discovered by Franken et al. [1], when a ruby laser was employed to illuminate quartz. This observation opened a new research field and was followed by numerous studies of different materials. In 1968 Kurtz and Perry [2] extended the experimental method to studies of powdered samples.

The SHG powder method is an extremely sensitive approach to detect the absence of an inversion center in crystalline structures [2]. The advantage of the method is that only very small amounts of samples are required and that the measurements are fast. Hence, it is widely used to estimate the second harmonic coefficients and for a rapid classification of new materials. Examples of SHG studies of temperature induced phase transitions can be found in Dougherty and Kurtz [3], Kurtz and Perry [2], Miller and Savage [4], and Furusawa et al. [5]. It is also possible to distinguish centrosymmetric and noncentrosymmetric symmetry using piezoelectric, pyroelectric, and ferroelectric effects [6]. However, measurements of those effects are difficult to implement in high pressure experiments.

With respect to SHG measurements, crystals may be classified as either “centrosymmetric”, “phase matchable” or “non-phase matchable” [2]. In non-phase matchable crystals, the phases of the fundamental wave (the incident photon with the frequency ω) and the second harmonic wave (with the frequency 2ω) are not matched because the second-harmonic and the fundamental wave propagate with different phase velocities, corresponding to the refractive index and the directions of the second harmonic wave and the fundamental wave [7]. Therefore, the intensity of the generated SHG signal is usually many orders of magnitude lower than the intensity of the fundamental wave. In phase matchable crystals, effective conversions from incident photons to SHG are possible by an appropriate choice of crystal orientation and polarization of the fields, so that the refractive index for the incident and the generated photons are the same. Centrosymmetric crystals generate no SHG intensity. However, if the symmetry is broken locally, e.g. due to the presence of surfaces, strains or defects, nominally centrosymmetric crystals may show SHG. For example, SHG measurements have been presented for surfaces [8], nanocrystals [9] or $BaTiO_3$ [10]. Furthermore, crystals which belong to a centrosymmetric space group may have an acentric magnetic structure, and it has been shown by Fiebig et al. [11] that this then allows the detection of a

temperature dependent magnetic phase transition, for example in centrosymmetric Cr_2O_3, by observation of the temperature dependence of the SHG signal.

In contrast to the numerous temperature-dependent studies, high pressure studies have been presented much less often and there are only very few SHG studies at concomitantly high pressure and high temperature. All high pressure studies employ diamond anvil cells (DAC), as these allow us to study materials under extreme (pressure, temperature) conditions and provide optical access to the sample. A first pressure dependent SHG study in a DAC has been performed on quartz by Pinnick et al. [12]. Later, other studies demonstrated the possibility of SHG measurements for the detection of a pressure induced phase transition on three monoclinic organic compounds [13], for a phase transition from the zinc blende structure type to the rock salt structure type in ZnSe [14] and for a phase transition from the wurtzite structure type to the rock salt structure type in ZnO [15] and AlN [16]. The high pressure structure of phase IV of $HgBr_2$ has been determined from X-ray diffraction and the space group of this phase was confirmed by SHG [17]. Kupenko et al. [18] reported unknown high pressure phases of ammonia borane (BH_3NH_3) based on Raman spectroscopy and observed SHG signals up to 130 GPa. Furthermore it was shown that pressure-induced magnetic phase transitions can be detected by SHG [19].

At high p, T conditions, with $p = 45$ GPa and $T = 1670$ K, the SHG method was used to confirm the absence of an inversion center in a high pressure and temperature phase of CO_2 [20]. The possibility to determine the p, T phase boundaries for phases undergoing a transition between a centrosymmetric and an acentric phase has been demonstrated by us [16]. SHG measurements can also be used for the exploration of influence on the transition pressure. For example the influence of deviatoric stress and particle size on the transition pressure of ZnO and AlN is presented in Bayarjargal et al. [15, 21].

However, while the temperature dependence of the SHG tensor is well described [4, 5, 22, 23], the pressure dependent behavior of the SHG signal is not well understood [12, 15].

Here, we present the results of our investigation of the pressure dependent behavior of quartz and ice VII using powder SHG measurements. We discuss the pressure dependence of the SHG intensity using quartz, ZnO and KIO_3 as examples.

2 Second harmonic generation

In bulk materials, the linear polarisation per unit volume is given by

$$P_i^l = \varepsilon_0 \chi_{ij} E_j^\omega \tag{1}$$

where (i, $j = 1, 2, 3$), P_i^l is the bulk polarisation, ε_0 the vacuum permittivity, χ_{ij} the linear susceptibility, and E_j^ω is the electric field [7, 24]. For a description of a non-linear response Eq. (1) is expanded by non-linear contributions to the polarisation:

$$P_i^{nl} = \varepsilon_0 \chi_{ijk} E_j^\omega E_k^\omega + \varepsilon_0 \chi_{ijkl} E_j^\omega E_k^\omega E_l^\omega + \ldots \tag{2}$$

where χ_{ijk} is the second order susceptibility and χ_{ijkl} is the third order susceptibility. The second order term χ_{ijk} is responsible for frequency doubling or SHG. χ_{ijk} is a third-rank tensor and hence exists only in acentric crystals. Frequently, χ_{ijk} is replaced by the SHG tensor d_{ijk}^{SHG}, where $d_{ijk}^{\mathrm{SHG}} = \chi_{ijk}/2$. Third order terms, χ_{ijkl}, are required for the description of third harmonic generation.

Powder samples consist of a large number of randomly oriented crystals. Due to the random orientation, the total SHG intensity of powder samples is equal to the sum of the SHG intensity generated by each single particle. Kurtz and Perry [2] presented an expression for the SHG intensity $I^{2\omega}$ of powder samples as a function of the intensity I^ω of the fundamental beam, assuming no absorption:

$$I^{2\omega} \cong \frac{32\pi}{c} \left(\frac{64\pi I^\omega}{\lambda (n_\omega + 1)^2 (n_{2\omega} + n_\omega)} \right)^2 (d_{av}^{\mathrm{SHG}})^2 \frac{L l_c^2}{\bar{r}} \sin^2 \left(\frac{\pi}{2} \frac{\bar{r}}{l_c} \right) \tag{3}$$

where d_{av}^{SHG} is the angular average of the tensor components of d_{ijk}^{SHG}, λ is the wavelength, c the speed of light in vacuum, $\bar{r}$ the average particle size, L the sample thickness, l_c the average coherence length, and n_ω and $n_{2\omega}$ the refractive indices for the fundamental and second harmonic wave, respectively.

The average coherence length (l_c) is defined by Eq. (4):

$$l_c = \frac{\lambda}{4(n_{2\omega} - n_\omega)} \tag{4}$$

The dependence of the SHG intensity on the SHG coefficient d_{av}^{SHG}, average coherence length (l_c) and average particle size ($\bar{r}$) has important consequences. If non-phase matched crystals are smaller than l_c, according to Eq. (3) the SHG intensity will increase linearly, $I^{2\omega} \propto \bar{r}L$. If the crystals are larger than l_c the solution to Eq. (3) starts to oscillate. However in a powder with a typical

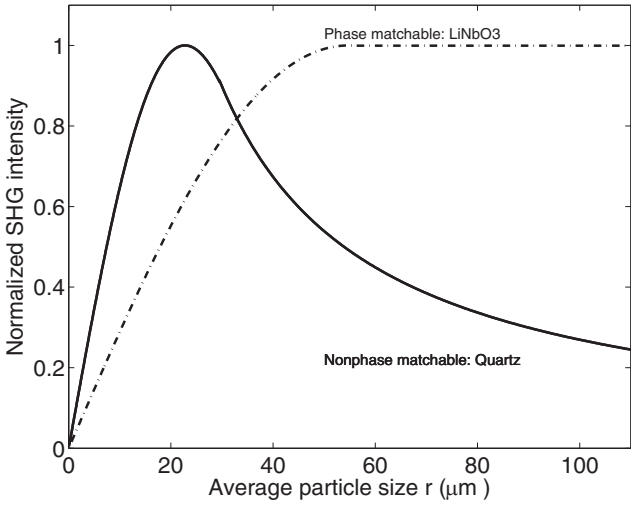

Fig. 1: Normalized SHG intensity of a powder sample as a function of average particle size $\bar{r}$ for phase matchable (dashed dot line, $LiNbO_3$) and non phase matchable crystals (solid line, α-SiO_2) was calculated using eqn. 3 from the refractive indices ($n_{\omega}^{1,SiO_2} = 1.533925$, $n_{\omega}^{3,SiO_2} = 1.54265$, $n_{2\omega}^{1,SiO_2} = 1.54652$, $n_{2\omega}^{3,SiO_2} = 1.5556$, $n_{\omega}^{1,LiNbO_3} = 2.23403$, $n_{\omega}^{3,LiNbO_3} = 2.15546$, $n_{2\omega}^{1,LiNbO_3} = 2.32513$ and $n_{2\omega}^{3,LiNbO_3} = 2.23315$ [37]). The corresponding calculated average coherence length of quartz is 30 μm.

particle size distribution the oscillations will not be observable [2]. Instead, the measured SHG intensity can then be described by the envelope of the oscillation and $I^{2\omega} \propto Ll_c^2/\bar{r}$. Equation (3) can be also used for a semi-quantitative estimation of the d_{av}^{SHG} values [2]. The possibility of a more accurate determination of SHG coefficients was demonstrated using samples with monolayers [25].

Due to the correlation between particle size and SHG intensity, measurements on samples with a range of grain sizes can be employed to distinguish between materials which are phase matchable and those which are not. Figure 1 illustrates as an example the correlation between SHG intensity and grain size for a non-phase matchable crystal (α-SiO_2) and a phase matchable crystal ($LiNbO_3$).

If for a phase matched crystal $\bar{r} \ll l_c$, the correlation between particle size and SHG intensity can be described by Eq. (3) and the SHG intensity will increase linearly $I^{2\omega} \propto \bar{r}L$. For large phase matched crystals ($\bar{r} \gg y_{PM}/\sin\theta_{PM}$) the SHG intensity will saturate and become independent of $\bar{r}$. The saturated SHG intensity is given by [2]:

$$I^{2\omega} \cong \frac{32\pi}{c}\left(\frac{64\pi I^{\omega}}{\lambda(n_{\omega}+1)^2(n_{2\omega}+n_{\omega})}\right)^2 (d_{PM}^{SHG})^2 \frac{\pi^2}{4} L\Gamma_{PM} \quad (5)$$

where $\Gamma_{PM} = \pi \frac{\sin\theta_{PM}}{\sin\rho}\frac{\lambda}{n}$, d_{PM}^{SHG} is the SHG tensor for phase matching, θ_{PM} is the phase matching angle and ρ is the angle between the Poynting vector and the wave vector.

3 Sample preparation and experimental setup

At ambient pressure it is possible to measure a non-compacted powder, a compacted powder or a powder which is immersed in a liquid of similar refractive index [2]. The latter technique leads to the decrease of the angular scattering, and the SHG intensity increases by one or two orders of magnitude. In DACs, SHG measurements can be performed with or without a pressure medium. If an inert gas is used as a pressure transmitting medium, it is useful to use a well compacted powder sample like that shown in Fig. 2. Alkali halides can be employed as a pressure medium to purposely induce shear on the sample at high pressures.

Some high pressure experiments have been made without any pressure-transmitting medium. For example, in the SHG measurements of CO_2 [20], and in our SHG measurements of ice VII described below, no pressure medium was employed. In these cases, the sample thickness is determined by the thickness of the gasket. For a conventional loading, where an inert gas is used as a pressure transmitting medium, a compacted sample with a typical thickness of 5–10 μm is preferable, depending whether or not the sample absorbs the laser light. For strongly absorbing samples it may be necessary to thermally insulate the sample from the diamond. There are established techniques, such as using an alkali halide layer or sapphire plates, which are employed for isolation for laser heating. However, it should be noted that heating of the sample by the laser may be a problem, especially if the transition temperature is close to the ambient temperature, as it is difficult to determine a temperature increase of few ten K in this set-up. Tunable laser sources or optical parametric oscillators can be used to overcome problems measuring absorbing samples or samples with a strong fluorescence.

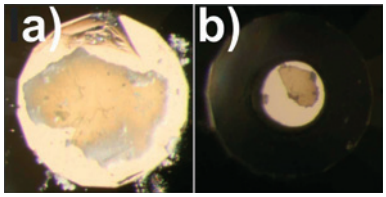

Fig. 2: a) Diamond anvils can be used to compact the powder samples. The picture shows compacted powder sample of ZnO on the diamond culet. b) A typical sample for SHG measurements. The picture shows the sample chamber containing ZnO and ruby in Ne at 1 GPa.

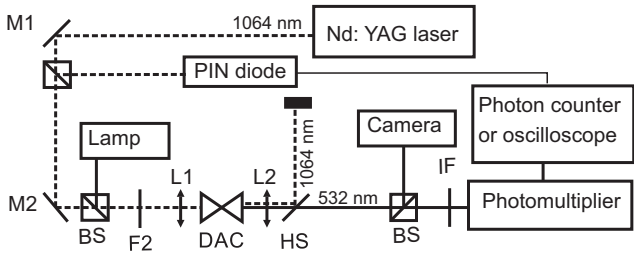

Fig. 3: The experimental set-up for powder SHG measurement. BS: beam splitter, |: mirrors, ↕: lens, F: filter, IF: interference filter, HS: SHG separator, DAC: diamond anvil cell with the sample. The dashed line presents the optical way of the fundamental beam. The continuous line presents the optical way of the SHG signal.

For our measurements, we usually employ Boehler-Almax [26] type diamond anvil cells. The typical diameters of our compacted samples are 20–50 μm and the sample thickness is typically around 5–10 μm. Samples are placed in gasket holes of about 110 μm diameter, which are drilled into pre-indented (to 40–50 μm thickness) tungsten gaskets. We determine the pressure using the ruby fluorescence method [27].

The layout of our experimental set-up for powder SHG measurements is shown in Fig. 3 [15]. While we employ a pulsed Nd:YAG or Nd:YLF lasers at 1064 or 1054 nm, respectively, other high powered lasers are equally suitable. For example, in the measurement of CO_2 at high pressures [20], a continuous Nd:YLF laser was employed, for both heating the sample and providing a fundamental wave for SHG. In our set-up the beam is split by a beam splitter, so that one part of the beam can be directed to the photodiode and serve as a trigger signal. The other beam passes through the DAC containing the sample. Harmonic separators or optical filters are used to separate the fundamental from the second harmonic signals (532 nm or 527 nm) behind the sample. The generated SHG signal is collected with a photo-multiplier. The photomultiplier signal and the trigger signal from the fundamental beam can also be displayed and detected using an oscilloscope. The description of a modified experimental set-up with laser heating can be found in Bayarjargal and Winkler [16].

The ratio of the sample signal to a reference signal should always be reported in a publication. It is therefore advisable to measure well known reference samples such as KH_2PO_4 (KDP), $LiNbO_3$, quartz (α-SiO_2) and Al_2O_3.

4 Examples

4.1 Phase transition of a non-phase matchable crystal: quartz (α-SiO_2)

At ambient pressure, most SHG efficiencies of powder non-phase matchable crystals are reported with respect to quartz. However, pressure dependent SHG measurements of quartz are important not only in the context of providing a reference, but also with respect to understanding the phase transformation of SiO_2 phases, which is still of fundamental importance for earth science, physics and chemistry.

Around 2 GPa, quartz transforms to coesite at equilibrium conditions [28]. At ambient temperature and at 15 GPa, quartz can start to amorphize [29]. The amorphization of quartz or coesite can also occur at higher pressures around 25–35 GPa [30]. However, a single crystal X-ray diffraction study of quartz (in argon) showed no pressure-induced amorphization up to 19.3 GPa [31]. At 21 GPa, the quartz II phase and new lines are observed in a nonhydrostatic pressure medium [32, 33]. The quartz II and the new phase with space group $P2_1/c$ appeared around 19–21 GPa in a quasihydrostatic pressure medium and both phases persisted stably up to 40 GPa [35]. Prakapenka et al. [34] detected that quartz transforms above 16 GPa to quartz II and above 22 GPa to a monoclinic structure with space group $P2_1/c$ without amorphization. Around 55 GPa, this monoclinic structure transforms to the $CaCl_2$ structure and at higher pressures to α-PbO_2 and to pyrite-type ($Pa\bar{3}$) structures [34].

Pinnick et al. [12] measured the phase transition of quartz with SHG and Raman experiments. A 4:1 methanol-ethanol mixture was used as a pressure-transmitting medium. Their measurements show a slight pressure-dependent decrease ($-0.3\%\ GPa^{-1}$) of the SHG intensity up to ≈22 GPa. Above 22 GPa the SHG intensity decreases drastically. However SHG intensity was still observed up to 31 GPa. This SHG signal was interpreted by Pinnick et al. [12] as an indication of the transformation between quartz I and quartz II.

We investigated the phase transformation of quartz by SHG up to 23.7 GPa in KCl. Our data are compared to the results by Pinnick et al. [12] in Fig. 4. In our study and on increasing pressure up to 15.9 GPa the SHG intensity of quartz decreases with a slope of $-1.1\%\ GPa^{-1}$. Between 15.9 GPa and 21 GPa the SHG intensity drops from 0.9 nearly to zero. At 23.7 GPa the SHG intensity remains nearly zero and indicates a phase with an inversion center. Hence, in contrast to the earlier SHG study by Pinnick et al. [12], our measurements show a phase transi-

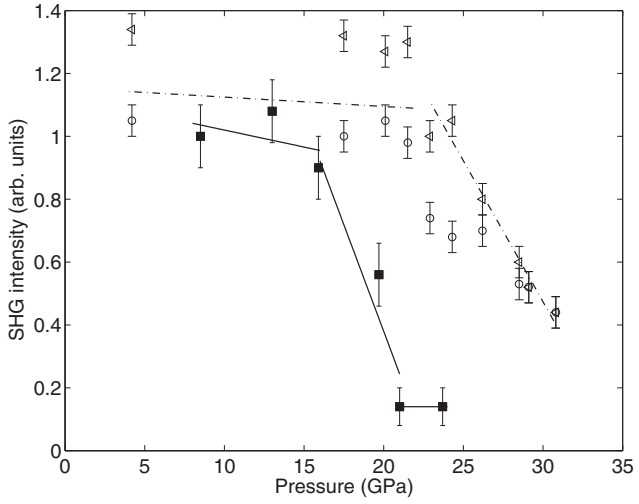

Fig. 4: The dark lines and dark squares present pressure dependence of the SHG intensity of α-SiO_2 in KCl on pressure increase in the current study. The dashed lines and open symbols represent the data from [12]. Open circles and triangles refer to two different polarizations of the incident laser beam.

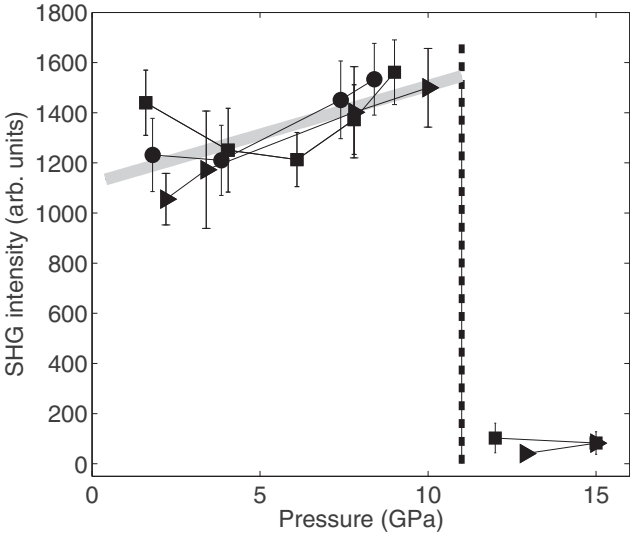

Fig. 5: Pressure dependence of the SHG intensity of ZnO on pressure increase. Different symbols represent the three different loadings in a 4:1 mixture of methanol and ethanol. The thick grey line represents a linear fit ($I_{SHG}^{ZnO} = (1.12 + 0.039 \cdot P) \cdot 1000$) of the pressure dependence of the SHG signal [15].

tion which can be related to either the complete amorphization [29] or to a transformation into the centrosymmetric structure $P2_1/c$ [35]. The difference between the two measurements can be attributed to the different pressure media employed. It would now be interesting to study the behavior in a hydrostatic pressure medium and add temperature as an additional variable. Such measurements are currently in progress.

4.2 Phase transition of non-phase matchable crystals: AlN and ZnO

AlN and ZnO are isostructural to wurtzite at ambient conditions, i.e. have the hexagonal, acentric B4 structure type. At ambient temperature and high pressure, they transform into phases with the rocksalt (B1) structure-type. These phase transitions were studied with SHG up to a pressure of 35 GPa in different pressure media [15, 16]. Both compounds show a similar evolution of the SHG intensity with pressure and a typical pressure dependence of the SHG intensity is shown in Fig. 5. On increasing pressure the SHG intensity increases, and then drops to zero at the phase transition. The pressure dependent SHG signal of ZnO has a slope of 3.9% GPa^{-1}. The difference between the two compounds is that the B4 phase of ZnO transforms rapidly into the B1 phase while the transition of AlN is sluggish and both polymorphs of AlN can coexist over a broad pressure range.

Depending on the pressure conditions, it has been suggested that ZnO can go through an acentric tetragonal intermediate *iT* (*I*4*mm*) phase, or a centrosymetric hexagonal intermediate *iH* ($P6_3/mmc$) phase at ambient temperature [36]. The SHG experiments of ZnO in a non-hydrostatic pressure medium show a decrease of the intensity of the SHG signal between 6–9 GPa [15]. This decrease of the SHG intensity has been interpreted by us to indicate the presence of the centrosymmetric *iH* phase. On the other hand, the positive slope of the intensity of the SHG signal in a hydrostatic pressure medium is due to the formation of an acentric tetragonal intermediate phase *iT*. These studies profited from the very large SHG coefficients (11.7 and 5.6 pm/V for AlN and ZnO, respectively) which are 20–40 times larger than quartz [37]. This advantage can be efficiently used for the determination of the phase boundaries at high pressure and temperature [16].

4.3 Phase transition of H_2O (ice VII)

Ice VII has space group $Pn\bar{3}m$ and exists at $P > 2.1$ GPa at ambient temperature [38]. Around 13–15 GPa, Raman measurements [39] of ice VII have shown a minimum in the linewidth of the $\nu_1(A_{1g})$ mode, which was thought to be correlated with a change in the ordering of the protons. During this pressure-induced change, a new low-frequency band appears at 150 cm^{-1} [40]. This phase transition of ice VII was investigated by X-ray diffraction by So-

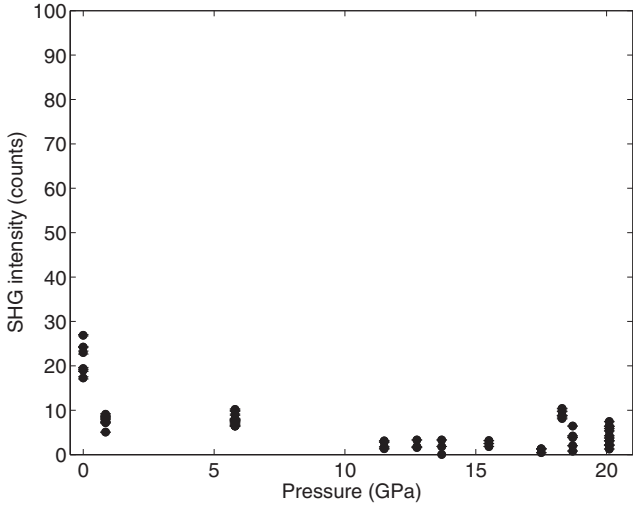

Fig. 6: Pressure dependence of the SHG signal of H_2O (ice VII) on compression.

mayazulu et al. [41], who observed a splitting of diffraction lines. They suggested the occurrence of spontaneous deformations near 14 GPa and a decrease of the symmetry from $Pn\bar{3}m$ to a lower acentric space group $P4_222$.

In order to further characterize this phase transition, we performed SHG experiments on ice VII (Fig. 6). On pressure increase, the SHG intensity of ice VII remains nearly zero up to 20.1 GPa. The reference quartz signal was around 350 counts and the ratio between the SHG signal of ice VII and the reference is $\sim$1/35. This indicates that the structure of ice VII is either centrosymetric or acentric with a very low SHG coefficient. To exclude the possibility of a acentric structure with a very low SHG coefficient, measurements with different filters or at different laser power can be employed. Any SHG signal can be separated from the background as it depends on the laser power, while the background is independent of the laser power. By variation of the laser power one can reach a very high sensitivity and measure SHG signals with intensities $<$ 1/1000 of a corresponding quartz signal [3]. At ambient conditions we increased the laser power so that the SHG signal was 2200–4500 counts for quartz (Fig. 7a). With the same increased laser power the SHG intensity of ice VII was measured at 20.1 GPa. The data are presented in (Fig. 7b). The ratios of the SHG intensity of the sample to that quartz are between 1/220 and 1/450. According the Eq. (3), the SHG intensity is proportional to the intensity of the fundamental beam $I^{2\omega} \propto I^{\omega}$. Hence the SHG intensity will increase for increasing laser power for noncentrosymmetric materials (Fig. 7a). Centrosymetric Al_2O_3 and ice VII at 20.1 GPa did not show any correlation between the SHG signal and

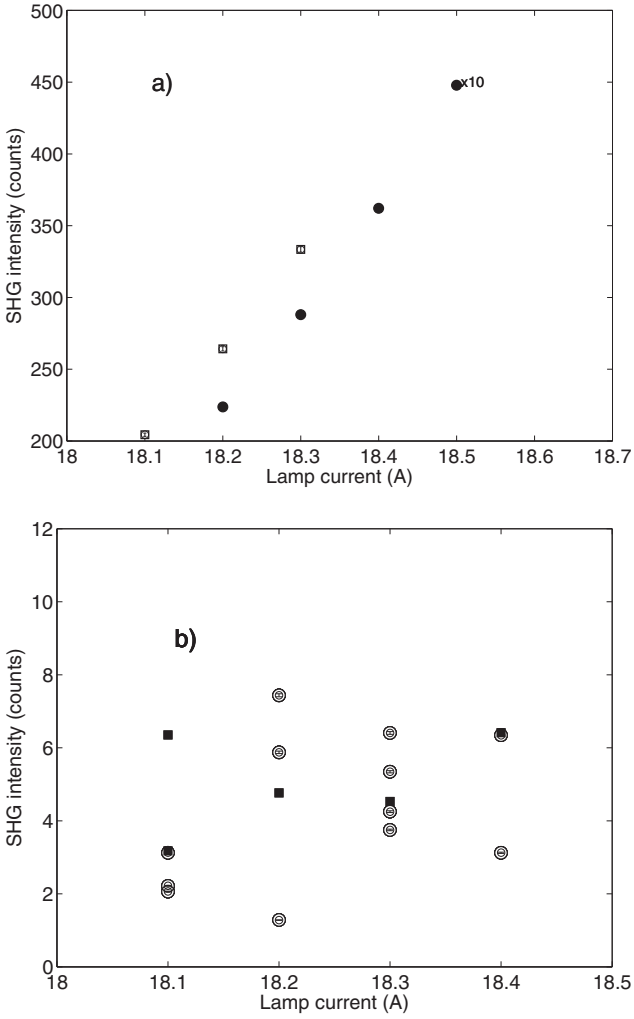

Fig. 7: a) Open squares represent the SHG measurements of the noncentrosymetric quartz at ambient conditions. Black circles represent the SHG measurements of noncentrosymetric quartz at ambient conditions with increased laser power (the intensity is 10 time higher that represented by the open squares). The laser power is linearly related to the lamp current. b) The SHG measurements of centrosymetric Al_2O_3 (black squares) was performed at ambient conditions and the SHG measurements of ice VII (circles) was performed with the increased laser power at 20.1 GPa. The laser power for ice VII (circles)was the same as for the quartz data (black circles) in Fig. 7a.

the laser power (Fig. 7b), and hence we conclude that if there is a phase transition in ice VII, the new polymorph has a centrosymetric structure above 14 GPa. The acentric space group suggested earlier [41] can be ruled out.

4.4 Phase transition of phase matchable crystal: KIO_3

At ambient conditions KIO_3 crystallizes in space group $P1$. KIO_3 is a phase matchable crystal and shows signifi-

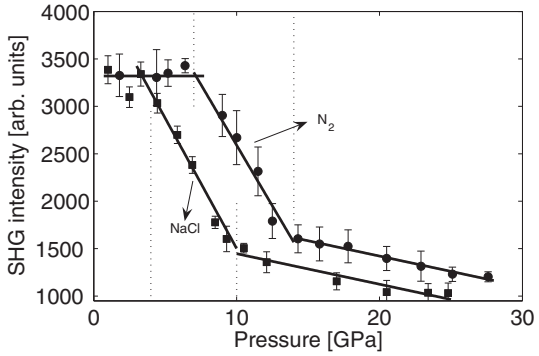

Fig. 8: The pressure dependence of the SHG signal of KIO_3 in a quasi-hydrostatic (nitrogen, circles) and a non-hydrostatic (NaCl, squares) pressure medium. It shows two pressure-induced structural phase transitions at 7 GPa and at 14 GPa (nitrogen) [44].

cant non-linear optical effects [42, 43]. Due to the low symmetry, crystal growth and the characterization of physical properties are difficult.

From SHG measurements, it became obvious that around 7 GPa KIO_3 transforms to a first acentric high pressure phase and at 14 GPa there is a second pressure-induced structural phase transition [44] (Fig. 8). The presence of strong SHG signals shows that all high pressure phases are acentric. The high-pressure behaviour of KIO_3 was then studied up to 30 GPa using X-ray diffraction, Raman spectroscopy, density functional-theory based calculations and SHG experiments [44] and the crystal structure of the first high pressure phase was solved from single crystal X-ray diffraction experiments. While the structure of the second high pressure phase currently is unsolved, it is clear that it is an acentric structure. The influence of the deviatoric stress on the transition is significant and can be easily determined using SHG [44].

5 Discussion and conclusion

We have demonstrated here that the pressure dependence of SHG intensities of non-phase matchable crystals can differ qualitatively. For quartz, we observed a pressure-induced decrease (Fig. 4) while for ZnO the SHG signal increases on increasing pressure (Fig. 9). To understand which factors determine whether there will be a negative or positive pressure dependence, we calculated the normalized SHG intensity of powder samples as a function of average particle size $\bar{r}$ for ZnO and quartz using Eq. (3) (Fig. 9). In DAC experiments, the sample thickness is around 5–10 μm, which is smaller than the average coherence length of quartz, as quartz has an average coherence length (l_c) of 30 μm (Fig. 1). Hence ac-

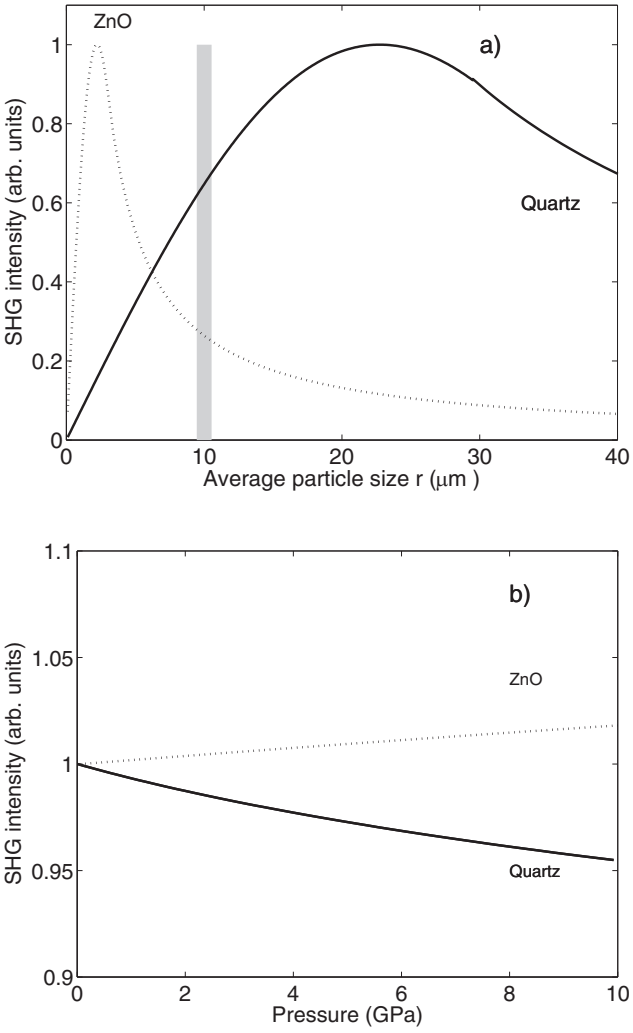

Fig. 9: a) Relative SHG intensity of a powder sample as a function of average particle size $\bar{r}$ was calculated for quartz (solid line) and ZnO (dashed line) using Eq. (3) from the refractive indices(($n_\omega^{1,ZnO}$ = 1.94042, $n_\omega^{3,ZnO}$=1.95502, $n_{2\omega}^{1,ZnO}$=2.02904, $n_{2\omega}^{3,ZnO}$=2.04636 [37]). The calculated average coherence length of ZnO is 3 μm. The shaded grey area delineates approximately the area (Fig. 9b) for which the pressure dependence of the SHG signal was calculated taking into account the bulk moduli. b) Calculated relative SHG intensity of a ZnO (dashed line) and quartz (solid line) as a function of the pressure.

cording to equation 3, the SHG intensity of quartz is proportional to $I^{2\omega} \propto Ll_c^2/r$ and decreases with decreasing particle size. In contrast to this, the average coherence length of ZnO is 3 μm and is smaller than the average particle size. Hence the SHG intensity will increase linearly by $I^{2\omega} \propto \bar{r}L$. In other words, the ratio between the average coherence length and the average particle size determines the slope of the pressure dependence of the SHG signal of non-phase matchable crystals.

In Fig. 9a), the shaded area around 10 μm delineates approximately the area for which the pressure depend-

ence of the SHG signal was calculated more accurately. For the accurate calculation (Fig. 9b) we considered that the crystals have an average particle size 10 μm at 0 GPa, but will become smaller due to compression. Taking into account the corresponding bulk moduli $B_{ZnO} = 183(7)$ GPa [45] and $B_{SiO_2} = 38.7$ GPa [31] the average particle sizes at 10 GPa are $\bar{r}_{ZnO} = 9.95$ μm and $\bar{r}_{SiO_2} = 9.90$ μm. For quartz, the calculation gives a slope of -0.4% GPa^{-1} in good agreement with the experimental values of -0.3% GPa^{-1} [12] and -1.1% GPa^{-1}. For ZnO the model calculations yielded a slope of 0.2% GPa^{-1}, which is one order of magnitude smaller than the experimentally determined value of 3.9% GPa^{-1}. Hence, the pressure dependence of SHG signal of quartz can be completely explained by the influence of the particle size while this is not the case for the pressure dependence of the SHG signal of ZnO. However, the ratio between the the average coherence length and the average particle size of ZnO defines the sign of the slope.

According to Fig. 1 and Eq. (4) the SHG intensity of a phase matchable crystal will decrease or remains constant for decreasing particle size. The example of the phase matchable crystal of KIO_3 shows that on pressure increase the SHG intensity did not change up to the first phase transition and then drops continuously (Fig. 8). Therefore the slope of pressure dependence of the SHG intensity depends also on the ratio between the the average coherence length and the average particle size of phase matchable crystals.

In summary, we performed SHG experiments in non-phase matchable crystals and phase matchable crystal and explained the observed pressure dependence of the SHG intensity with the correlation of the average particle size. We have shown that SHG is an efficient and accurate tool for the detection of phase transitions between centrosymmetric and acentric phases. It is a laboratory based technique, which can be employed for high pressure studies at low, ambient and high temperatures. It is complementary to X-ray diffraction as it provides additional information about the presence of an inversion center. With the availability of optical parametric oscillators or other tools to provide tunable laser light, it can be employed also for strongly absorbing samples. Hence we believe that this technique will become increasingly useful in studies of structure-property relations in the near future.

Acknowledgement: Financial support from the DFG, Germany, within SPP1236 (projects Ba-4020, WI-1232) and the FOKUS program of the Goethe University is gratefully acknowledged.

References

[1] Franken, P. A.; Hill, A. E.; Peters, C. W.; Weinreich, G.: Generation of optical harmonics. Phys. Rev. Lett. **7** (1961) 118–119.
[2] Kurtz, S. K.; Perry, T. T.: A powder technique for the evaluation of nonlinear optical materials. J. Appl. Phys. **39** (1968) 3798–3813.
[3] Dougherty, J. P.; Kurtz, S. K.: A second harmonic analyzer for the detection of non-centrosymmetry. J. Appl. Cryst. **9(2)** (1976) 145–158.
[4] Miller, R. C.; Savage, A.: Temperature dependence of the optical properties of ferroelectric $LiNbO_3$ and $LiTaO_3$. Appl. Phys. Lett. **9(4)** (1966) 169–171.
[5] Furusawa, S.; Chikagawa, O.; Tange, S.; Ishidate, T.; Orihara, H.; Ishibashi, Y.; Miwa, K.: Second Harmonic Generation in $Li_2B_4O_7$. J. Phys. Soc. Jpn. **60** (1991) 2691–2693.
[6] Ok, K. M.; Chi, E. O.; Halasyamani, P. S.: Bulk characterization methods for non-centrosymmetric materials: second-harmonic generation, piezoelectricity, pyroelectricity, and ferroelectricity. Chem. Soc. Rev. **35** (2006) 710–717.
[7] Boyd, R. W.: Nonlinear Optics. Academic Press, San Diego (2003).
[8] Suzuki, T.; Mikami, A.; Kimura, Y.; Uehara, K.; Aono, M.: Optical method for investigation of the kinetics of the Si(111) phase transition. Surf. Sci. **357** (1996) 107–110.
[9] Ray, P. C.: 2010. Size and shape dependent second order nonlinear optical properties of nanomaterials and its application in biological and chemical sensing. Chem. Rev. **110(9)** (2010) 5332.
[10] Pugachev, A. M.; Kovalevskii, V. I.; Surovtsev, N. V.; Kojima, S.; Prosandeev, S. A.; Raevski, I. P.; Raevskaya, S. I.: Broken Local Symmetry in Paraelectric $BaTiO_3$ Proved by Second Harmonic Generation. Phys. Rev. Lett. **108** (2012) 247601.
[11] Fiebig, M.; Fröhlich, D.; Krichevtsov, B. B.; Pisarev, R. V.: Second Harmonic Generation and Magnetic-Dipole-Electric-Dipole Interference in Antiferromagnetic Cr_2O_3. Phys. Rev. Lett. **73** (1994) 2127–2130.
[12] Pinnick, D. A.; Lee, S. A.; Sun, X.; Simon, H. J.: Optical second-harmonic-generation study of quartz up to 31 GPa. Phys. Rev. B **55** (1997) 8031–8033.
[13] Li, Y.; Yang, G.; Dreger, Z. A.; White, J. O.; Drickamer, H. G.: Effect of high pressure on the second harmonic generation efficiencies of three monoclinic organic compounds. J. Phys. Chem. **102(31)** (1998) 5963–5968.
[14] Jin, M.; Cui, Q.; Mukhtar, E.; Ding, D.: Second harmonic generation measurements on ZnSe under high pressure. J. Phys.: Condens. Matter **14** (2002) 11037–11040.
[15] Bayarjargal, L.; Winkler, B.; Haussühl, E.; Boehler, R.: Influence of deviatoric stress on the pressure-induced structural phase transition of ZnO studied by optical second harmonic generation measurements. Appl. Phys. Lett. **95** (2009) 061907.
[16] Bayarjargal, L.; Winkler, B.: High (pressure, temperature) phase diagrams of ZnO and AlN from second harmonic generation measurements. Appl. Phys. Lett. **100** (2012) 021909.
[17] Hostettler, M.; Schwarzenbach, D.; Helbing, J.; Dmitriev, V.; Weber, H. P.: Structure and SHG of the high pressure phase IV of $HgBr_2$. Solid State Commun. **129**(6) (2004) 359–363.
[18] Kupenko, I.; Dubrovinsky, L.; Dmitriev, V.; Dubrovinskaia, N.: In situ Raman spectroscopic study of the pressure induced

structural changes in ammonia borane. J. Chem. Phys. **137(7)** (2012) 074506.
[19] Bayarjargal, L.; Winkler, B.: Pressure-induced magnetic phase transition in Cr_2O_3 determined by second harmonic generation measurements. Appl. Phys. Lett. **102** (2013) 182403.
[20] Iota, V.; Yoo, C. S.; Cynn, H.: Quartzlike Carbon Dioxide: An Optically Nonlinear Extended Solid at High Pressures and Temperatures. Science **283(5407)** (1999) 1510–1513.
[21] Bayarjargal, L.; Wiehl, L.; Winkler, B.: Influence of grain size, surface energy, and deviatoric stress on the pressure induced phase transition of ZnO and AlN. High Pressure Res. **33** (2013) 642–651.
[22] Vogt, H.: Study of structural phase transitions by techniques of nonlinear optics. Appl. Phys. A: Mater. Sci. Process. **5(2)** (1974) 85–96.
[23] Miller, R. C.; Nordland, W. A.; Bridenbaugh, P. M.: Dependence of Second-Harmonic-Generation Coefficients of $LiNbO_3$ on Melt Composition. J. Appl. Phys. **42(11)** (1971) 4145–4147.
[24] Sutherland, R. L.: Handbook of nonlinear optics. Vol. 82. CRC (2003).
[25] Aramburu, I.; Ortega, J.; Folcia, C. L.; Etxebarria, J.; Illarramendi, M. A., Breczewski, T.: Accurate determination of second order nonlinear optical coefficients from powder crystal monolayers. J. Appl. Phys. **109** (2011) 113105.
[26] Boehler, R.: New diamond cell for single-crystal X-ray diffraction. Rev. Sci. Instrum. **77** (2006) 115103.
[27] Mao, H. K.; Bell, P. M.; Shaner, J. W.; Steinberg, D. J.: Specific volume measurements of Cu, Mo, Pd and Ag and calibration of the ruby R1 fluorescence pressure gauge from 0.06 to 1 Mbar. J. Appl. Phys. **49** (1978) 3276–3283.
[28] Bohlen, S. R.; Boettcher, A. L.: The quartz ⇌ coesite transformation: A precise determination and the effects of other components. J. Geophys. Res. **87** (1982) 7073–7078.
[29] Kingma, K. J.; Meade, C.; Hemley, R. J.; Mao, H. K.; Veblen, D. R.: Microstructural observations of α-quartz amorphization. Science **259** (1993) 666–669.
[30] Hemley, R. J.; Jephcoat, A. P.; Mao, H. K.; Ming, L. C.; Manghnani, M. H.: (1988) Pressure-induced amorphization of crystalline silica. Nature **334** (6177) (1988) 52–54.
[31] Kim-Zajonz, J.; Werner, S.; Schulz, H.: High pressure single crystal X-ray diffraction study on α-quartz. Z. Kristallogr. **214(6)** (1999) 324–330.
[32] Kingma, K. J.; Hemley, R. J.; Mao, H. K.; Veblen, D. R.: New high-pressure transformation in α-quartz. Phys. Rev. Lett. **70** (1993) 3927–3930.
[33] Kingma, K. J.; Mao, H. K.; Hemley, R. J.: Synchrotron X-ray diffraction of SiO_2 to multimegabar pressures. High Pressure Res. **14(4–6)** (1996) 363–374.
[34] Prakapenka, V. P.; Shen, G.; Dubrovinsky, L. S.; Rivers, M. L.; Sutton, S. R.: High pressure induced phase transformation of SiO_2 and GeO_2: difference and similarity. J. Phys. Chem. Solids **65(8)** (2004) 1537–1545.
[35] Haines, J.; Léger, J. M.; Gorelli, F.; Hanfland, M.: Crystalline post-quartz phase in silica at high pressure. Phys. Rev. Lett. **87(15)** (2001) 155503.
[36] Boulfelfel, S. E.; Leoni, S.: Competing intermediates in the pressure-induced wurtzite to rocksalt phase transition in ZnO. Phys. Rev. B **78** (2008) 125204.
[37] Charra, F.; Gurzadyan, G.: Landolt-Börnstein, Group III, High Frequency Properties of Dielectric Crystals. Vol. 30. Springer Verlag, Berlin (2000).
[38] Wolanin, E.; Pruzan, P.; Chervin, J. C.; Canny, B.; Gauthier, M.; Häusermann, D.; Hanfland, M.: Equation of state of ice VII up to 106 GPa. Phys. Rev. B **56** (1997) 5781–5785.
[39] Pruzan, P.; Chervin, J. C.; Wolanin, E.; Canny, B.; Gauthier, M.; Hanfland, M.: Phase diagram of ice in the VII-VIII-X domain. Vibrational and structural data for strongly compressed ice VIII. J. Raman Spectrosc. **34(7–8)** (2003) 591–610.
[40] Yoshimura, Y.; Stewart, S. T.; Somayazulu, M.; Mao, H. K.; Hemley, R. J.: Convergent Raman features in high density amorphous ice, ice VII, and ice VIII under pressure. J. Phys. Chem. B **115(14)** (2011) 3756–3760.
[41] Somayazulu, M.; Shu, J.; Zha, C. S.; Goncharov, A. F.; Tschauner, O.; Mao, H. K.; Hemley, R. J.: In situ high-pressure X-ray diffraction study of H_2O ice VII. J. Chem. Phys. **128(6)** (2008) 064510.
[42] Bergman, J. G.; Boyd, G. D.; Ashikin, A.; Kurtz, S. K.: New Nonlinear Optical Materials: Metal Oxides with Nonbonded Electrons. J. Appl. Phys. **40** (1969) 2860.
[43] Xin, Y.; Mengkai, L.; Shaojun, Z.; Fuqi, L.: Nonlinear optical properties of perfectly polarized KIO_3 single crystal. Chinese Phys. Lett. **9** (1992) 77.
[44] Bayarjargal, L.; Wiehl, L.; Friedrich, A.; Winkler, B.; Juarez-Arellano, E. A., Morgenroth, W.; Haussühl, E.: Phase transition in KIO_3. J. Phys.: Condens. Matter **24** (2012) 325401.
[45] Karzel, H.; Potzel, W.; Kofferlein, M.; Schiessl, W.; Steiner, M.; Hiller, U., Kalvius, G. M.; Mitchell, D. W.; Das, T. P.; Blaha, P.; Schwarz, K., Pasternak, M. P.: Lattice dynamics and hyperfine interactions in ZnO and ZnSe at high external pressures. Phys. Rev. B **53** (1996) 11425.

Received April 6, 2013; accepted May 30, 2013
Published online February 5, 2014